International Journal of Nanomedicine

Dovepress

open access to scientific and medical research

Open Access Full Text Article

ORIGINAL RESEARCH

Existence, release, and antibacterial actions of silver nanoparticles on Ag–PIII TiO_2 films with different nanotopographies

This article was published in the following Dove Press journal:
International Journal of Nanomedicine
16 July 2014
Number of times this article has been viewed

Jinhua Li
Yuqin Qiao
Hongqin Zhu
Fanhao Meng
Xuanyong Liu

State Key Laboratory of High Performance Ceramics and Superfine Microstructure, Shanghai Institute of Ceramics, Chinese Academy of Sciences, Shanghai, People's Republic of China

Abstract: Nanotopographical TiO_2 films (including nanorod, nanotip, and nanowire topographies) were successfully fabricated on the metallic Ti surface via hydrothermal treatment and then underwent Ag plasma immersion ion implantation to incorporate Ag with TiO_2. The surface morphology, phase component, and chemical composition before and after Ag–PIII were characterized. In view of the potential clinical applications, both Gram-negative *Escherichia coli* and Gram-positive *Staphylococcus aureus* were used to estimate their antimicrobial effect. The nanostructured TiO_2 films on a Ti surface exhibit a better bacteriostatic effect on both microbes compared to the pristine Ti. The nanotopographies of the TiO_2 films affect the nucleation, growth, and distribution of Ag nanoparticles in the films during Ag–PIII process. The Ag nanoparticles are completely embedded into the nanorod film while partially exposed out of the nanotip and nanowire films, which account for the significant differences in the release behaviors of Ag ions in vitro. However, no significant difference exists in their antimicrobial activity against both microbes. The antimicrobial actions of the Ag@TiO_2 system described here consist of two methods – the contact-killing action and the release-killing action. Nevertheless, based on the observed results, the contact-killing action should be regarded as the main method to destroy microbes for all the Ag plasma-modified TiO_2 nanofilms. This study provides insight to optimize the surface design of Ti-based implants to acquire more effective antimicrobial surfaces to meet clinical applications.

Keywords: silver, nanoparticles, titania, nanostructure, antibacterial, plasma

Introduction

Nanotechnology has the powerful capability to integrate nanobionics into materials science and engineering. Hence, a great deal of interest has been paid to the investigations on nanostructured/nanofunctionalized biomaterials. The biological effects of a nanofeatured surface can be enhanced, and the clinical applications of biomedical materials can be promoted.[1] It is widely accepted that, once being implanted into the human body, a range of interactions emerges at the interface of the biomaterials surface and the physiological environment. Hence, the surface of biomaterials plays a crucial role in the response of artificial implants to the physiological environment. The performance of biomedical implant devices depends predominantly on the surface features, such as surface topography, microstructure, component, and resulting properties.[1]

Titanium-based implants are important to reinforce the human lifespan and its quality.[2] Nevertheless, bacteria tend to adhere on their surfaces and produce biofilms.[3] Actually, implant-associated failures are mainly caused by bacterial infections.[4,5] Once attaching upon the implants, the microbes proliferate and assemble to generate biofilms and, subsequently, trigger tissue infection.[6] It is a general

Correspondence: Xuanyong Liu
State Key Laboratory of High Performance Ceramics and Superfine Microstructure, Shanghai Institute of Ceramics, Chinese Academy of Sciences, 1295 Ding-xi Road, Shanghai 200050, People's Republic of China
Tel +86 21 524 124 09
Email xyliu@mail.sic.ac.cn

submit your manuscript | www.dovepress.com
Dovepress
http://dx.doi.org/10.2147/IJN.S63807

strategy to load antibiotics onto implant surfaces to reduce infections.[4] Nowadays, however, a great deal of attention has been paid to the antibiotic-resistant bacteria, some of which has produced intractable resistance by using existing antibiotics.[7] In view of such circumstances, it is a development trend to endow implant materials/devices with self-antibacterial performance to inhibit bacterial attachment and resultant infections.[8,9]

TiO_2 can inhibit microbe adhesion due to its excellent photocatalytic activity.[10–12] Nevertheless, this function will inevitably attenuate in darkness, for example, in the human body.[13,14] Furthermore, to cure persistent infections, it is a promising antibacterial method to damage the membrane functions of bacteria.[15,16] Ag (including nanoparticle, ion, and metal) has the powerful ability to fight against a wide spectrum of bacteria and fungi, owing to its nonspecific antibacterial skill.[8,17,18] In addition, the possibility that Ag-resistant microbes will come out in the future seems remote indeed over a period of time.[19] It is considered that Ag nanoparticles are rather more reactive than bulk Ag metal, owing to a large reactive specific surface area. Thus, kinds of Ag nanoparticle-modified surfaces have been designed and prepared.[20–22]

Plasma immersion ion implantation (PIII) technology has now been extensively utilized to modify the surfaces of a variety of biomedical materials/devices and found especially suitable for the ones with complex geometry shapes, due to the non-line-of-light feature.[23] The Ag–PIII method has been successfully developed for the purpose of enhancing the antibacterial ability of biomaterials and related devices to minimize infections.[24] Nowadays, the Ag–PIII technique has been broadly attempted to modify polymer-based biomaterials[25–27] and titanium-based biomaterials.[28,29] The growth habit of the Ag nanoparticles within the TiO_2 matrix obeys the classical nucleation theory when Ag plasma interacts with TiO_2 film.[30] The topographies of TiO_2 films also influence the distribution of electric field and plasma sheath around TiO_2 films.[31]

In the present work, nanostructured TiO_2 films (including nanorod, nanotip, and nanowire topographies) were prepared on a titanium surface via hydrothermal method to obtain nanotopographies and subsequently treated by PIII procedure to incorporate with Ag nanoparticles. The effect of TiO_2 nanotopographies on the growth habit of Ag nanoparticles in TiO_2 films was discussed. The influence of Ag plasma-modified TiO_2 nanofilms on microbes (*Escherichia coli* and *Staphylococcus aureus*) was evaluated.

Materials and methods

Preparation and modification of samples

Commercially pure titanium (Cp Ti) plates with sizes of 10×10×1 mm were ultrasonically cleaned in ethanol, deionized water, and ultrapure water three times for each. After that, they then underwent pickling in 5% weight oxalic acid solution at 100°C for 2 hours to eliminate the oxide layers and to obtain homogeneous surfaces. After that, the specimens were ultrasonically cleaned and dried in ambient atmosphere for further use. The TiO_2 nanostructures on titanium surface were hydrothermally fabricated. Briefly, the pretreated Ti plates were soaked in the mixed solution of hydrogen peroxide (30% weight H_2O_2) and sodium hydroxide (5 M NaOH) solution in Teflon-lined reaction vessels at a designated temperature and period (Table 1). After the reaction vessels cooling down, the Ti plates were gently cleaned with fresh water, dried, followed by protonation in dilute hydrochloric acid (0.1 M HCl) for 2 hours. After that, the samples were cleaned, dried, and finally heat-treated to obtain the nanostructured surfaces on titanium. And the as-obtained samples were designated as "nanorod," "nanotip," and "nanowire," respectively (Table 1).

The PIII technique was used to implant Ag into the nanotopographical titanium surfaces. The implantation parameters are listed in Table 2. The cathode rod was made of pure Ag metal with a purity of 99.99% weight and diameter of 10 mm. The ultimate samples were obtained and denoted as "Ag@nanorod", "Ag@nanotip", and "Ag@nanowire", respectively. The whole fabrication procedures are illustrated in Figure 1.

Surface characterization

The surface morphology was observed by field emission scanning electron microscopy (SEM; S-4800, Hitachi Ltd., Tokyo, Japan). The crystallinity of the films was characterized using an X-ray diffractometer (XRD; D/Max, Rigaku,

Table 1 Experimental details for the fabrication and modification of samples

	H_2O_2	NaOH	Hydrothermal treatment	Protonation	Calcination
Nanorod	10 mL		80°C for 72 hours		
Nanotip	7.5 mL	2.5 mL	80°C for 24 hours	0.1 M HCl for 2 hours	450°C for 1 hours
Nanowire		10 mL	80°C for 24 hours	0.1 M HCl for 2 hours	450°C for 1 hours

Table 2 Important instrumental parameters used in Ag–PIII

	Target	Cathodic arc
Voltage pulse duration (μs)	450	450
Pulsing frequency (Hz)	7	7
Ion implantation voltage (kV)	−15	
Ion implantation time (min)	30	
Pressure (Pa)	3.6×10^{-3}	

Abbreviation: PIII, plasma immersion ion implantation.

Tokyo, Japan) fitted with a Cu Kα (λ=1.541 Å) source at 40 kV and 100 mA in the range of 2θ=15°–80° with a step size of 0.02°. Phase identification was performed with the help of the standard Joint Committee on Powder Diffraction Standards database. During the X-ray diffraction test, the glancing angle of the incident beam against the sample surfaces was fixed at 1°. The chemical compositions and chemical states of the sample surfaces were investigated by X-ray photoelectron spectroscopy (XPS; PHI 5802, Physical Electronics Inc, Eden Prairie, MN, USA). At the same time, the transmission electron microscope (TEM) characterization was conducted on a field-emission TEM (JEM-2100F, JEOL, Tokyo, Japan) with an accelerating voltage of 200 kV. Specimens for the characterization were scratched off the surfaces and then dispersed in ethanol using ultrasound. A droplet of the suspension was located on a holey copper grid covered with porous carbon film (Quantifoil Micro Tools GmbH, Jena, Germany).

Ag ions release

The as-prepared Ag–PIII specimens were immersed in 10 mL fresh water at 37°C for 1 day, 3 days, and 7 days, successively. At the end of each immersion period, the leaching solution was gathered, and the release amount of Ag ions was determined by using inductively coupled plasma mass spectrometry (Nu Instruments Ltd, Wrexham, UK).

Antimicrobial efficiency determination

The antimicrobial activity on the Cp Ti, nano-TiO_2, and Ag–PIII samples was estimated by the microbial counting

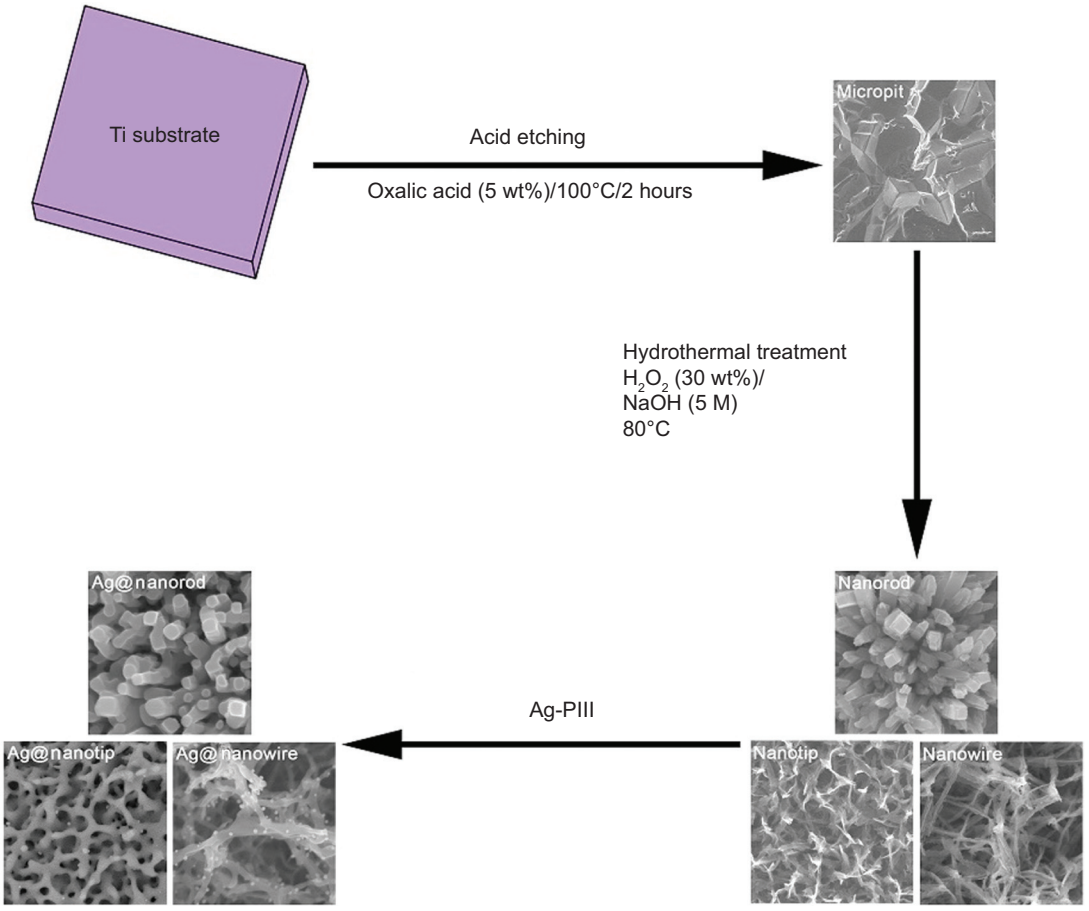

Figure 1 Schematic fabrication procedures of the nanostructured TiO_2 films loaded with Ag nanoparticles on Ti surface by combining acid etching, hydrothermal treatment, and processing together.
Abbreviations: PIII, plasma immersion ion implantation; wt, weight.

method using *E. coli* (*E. coli*, ATCC 25922; American Type Culture Collection [ATCC], Manassas, VA, USA) and *S. aureus* (*S. aureus*, ATCC 25923; American Type Culture Collection). The samples were sterilized in an autoclave at 121°C for 40 minutes. A solution containing the bacteria at a concentration of 10^7 colony-forming unit (CFU)/mL was introduced onto the sample to a density of 60 μL/cm^2. The samples with the microbial solution were incubated at 37°C for 24 hours. The dissociated microbial solution was collected and inoculated into a standard agar culture medium. After incubation at 37°C for 24 hours, the active bacteria were counted in accordance with the National Standards of the People's Republic of China GB/T 4789.2 protocol, and the antimicrobial ratio was calculated using the following formula,

$$\frac{(A-B)}{A}\times 100\%$$

where A is the average number of the bacteria on the control sample (CFU/sample); B is the average number of bacteria on the testing samples (CFU/sample).

In the SEM examination, a solution containing the bacteria at a concentration of 10^7 CFU/mL was put on the sample to a density of 60 μL/cm^2, incubated at 37°C for 24 hours, fixed, and dehydrated in a series of ethanol solutions (30%, volume–volume [v/v]; 50% v/v; 75% v/v; 90% v/v, 95% v/v; and 100% v/v) for 10 minutes each sequentially, with the final dehydration conducted in absolute ethanol (twice) followed by drying in the hexamethyldisilazane ethanol solution series.

Results and discussion

Characterization of samples

Figure 2 shows the surface morphology of Ti metal plates after undergoing the corresponding treatments. Compared to the rough Cp Ti surface (Figure 2A), three different architectures were obtained by altering the experimental parameters, as given in Figure 2C, E, and G. From the visual fields of SEM at high magnification, three types of nanowire, nanotip, and nanorod topographies (Figure 2D, F, and H, respectively) were generated when metallic Ti plates reacted in the corresponding hydrothermal conditions, while the Cp Ti presented a comparatively flat morphology at high magnification (Figure 2B).

From the XPS full spectra acquired in Figure 3A, it can be seen that only Ti and O elements existed on the surfaces of the nanorod, nanotip, and nanowire samples. From

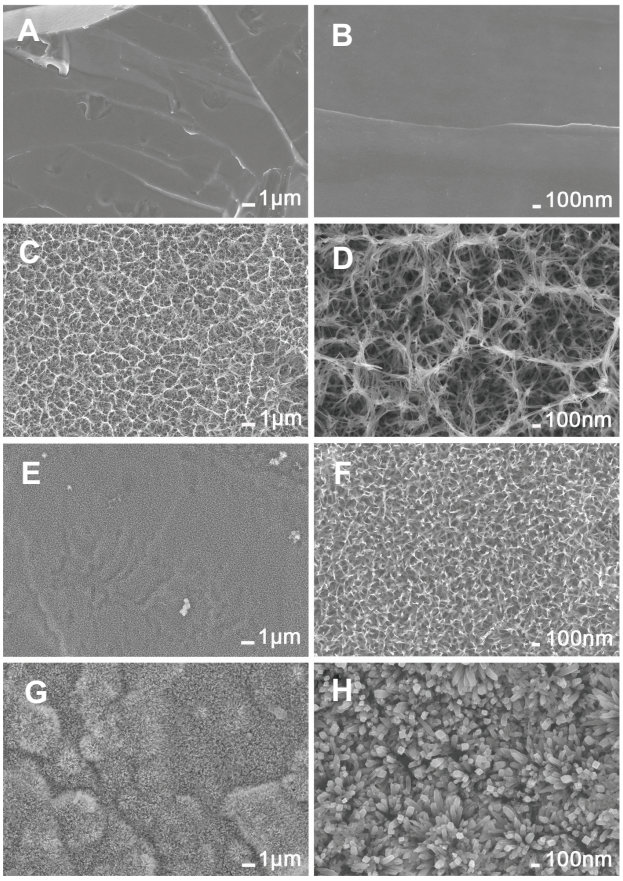

Figure 2 SEM morphology of the synthesized Cp Ti (**A**, **B**), nanowire (**C**, **D**), nanotip (**E**, **F**), and nanorod (**G**, **H**) at low- and high-magnification, respectively.
Abbreviations: SEM, scanning electron microscope; Cp, commercially pure.

Figure 3B, the XPS high-resolution spectra of Ti 2p contain two peaks centered at around 464.56 eV and 458.83 eV, which correspond to the typical binding energy for the Ti $2p_{1/2}$ and Ti $2p_{3/2}$ in TiO_2, respectively.[32,33] The peaks located at around 530.47 eV in Figure 3C are allotted to the O 1s in TiO_2.[34] In addition to the chemical components, it is also essential to identify the crystal structures of TiO_2 (including amorphous, anatase, rutile, brookite, or their mixed phases). The XRD data of the nanorod, nanotip and nanowire are revealed in Figure 3D. As can be clearly found from this figure, the crystal structure is the mixed phases of anatase and rutile.[35]

After the Ag–PIII process, the surface topographies seemed without significant change at low magnification (Figure 4A, C, and E). From the visual field of SEM at high magnification, the nanowire topography was damaged to some extent (Figure 4B); whereas, the nanotip topography was destroyed severely (Figure 4D). Furthermore, homogeneously distributed nanoparticles can be seen on the entire surfaces of both Ag@nanowire and Ag@nanotip (white

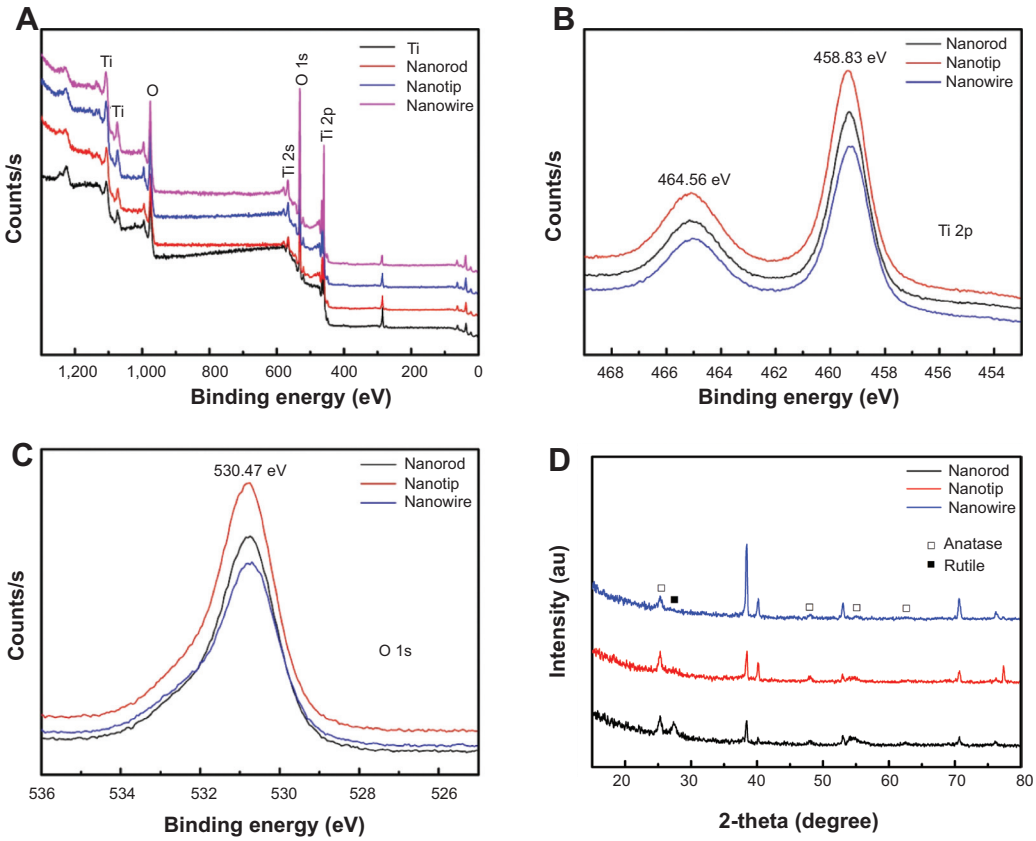

Figure 3 XPS full spectra (**A**), accompanied by the corresponding Ti 2p XPS spectra (**B**), O 1s XPS spectra (**C**), and XRD patterns (**D**) of the Cp Ti, nanowire, nanotip, and nanorod.

Abbreviations: XPS, X-ray photoelectron spectroscopy; XRD, X-ray diffractometer; CP, commercially pure; au, arbitrary units.

arrows in Figure 4B and D). On the contrary, the nanorod topography was not altered too much, and no nanoparticles were found on Ag@nanorod surface (Figure 4F). The XPS full spectra of all the Ag–PIII samples further indicated the presence of Ag element (Figure 5A). Figure 5B shows the XPS high-resolution Ag 3d spectra acquired from the Ag–PIII samples. The Ag 3d doublets at around 368.10 eV (Ag $3d_{5/2}$) and 374.10 eV (Ag $3d_{3/2}$) with a spin energy separation of 6.0 eV are assigned to metallic Ag,[36,37] demonstrating that the observed nanoparticles are metallic Ag.

To further testify the existing forms of metallic Ag on the three nanotopographical surfaces, the Ag–PIII specimens were characterized by the TEM method. The results are shown in Figure 6. Figure 6A gives the typical bright-field (BF) TEM view of Ag-implanted TiO_2 nanowires scratched off from the Ag@nanowire surface. From this figure, one can see abundant nanoparticles along the nanowires, which were demonstrated as Ag nanoparticles by the energy-dispersive X-ray spectroscopy (EDS) spectrum (Figure 6C, corresponding to the rectangular area in Figure 6A). The corresponding high-resolution transmission electron microscope image in Figure 6B clearly displays the existing forms of Ag nanoparticles on the nanowires. In detail, these nanoparticles are divided into two types. Some Ag nanoparticles are completely immersed in the TiO_2 nanowires, while other Ag nanoparticles are partially embedded in the nanowires with partially being exposed. Meanwhile, the high-resolution TEM image lattice patterns in Figure 6B further verify the nanoparticles are metallic Ag nanoparticles, and they possess excellent crystallinity. A similar situation exists in the Ag-implanted TiO_2 nanotips. Nevertheless, it is observed that the number of Ag nanoparticles on the nanotips (Figure 6D) is smaller than that of the former in Figure 6A. On the contrary, there are no Ag nanoparticles around the Ag-implanted TiO_2 nanorods, as shown in Figure 6G. Figure 6I depicts the corresponding EDS analysis result, obtained from the rectangular area in Figure 6G, which further certifies the existence of Ag element and agrees well with the XPS analysis result in Figure 5. From Figure 6H, one can find lots of tiny nanoparticles completely immersed in the TiO_2 nanorods. Obviously, these tiny nanoparticles are the Ag nanoparticles, which did not migrate to the nanorod surface during the Ag–PIII process. These observed results imply that the nanotopographies of

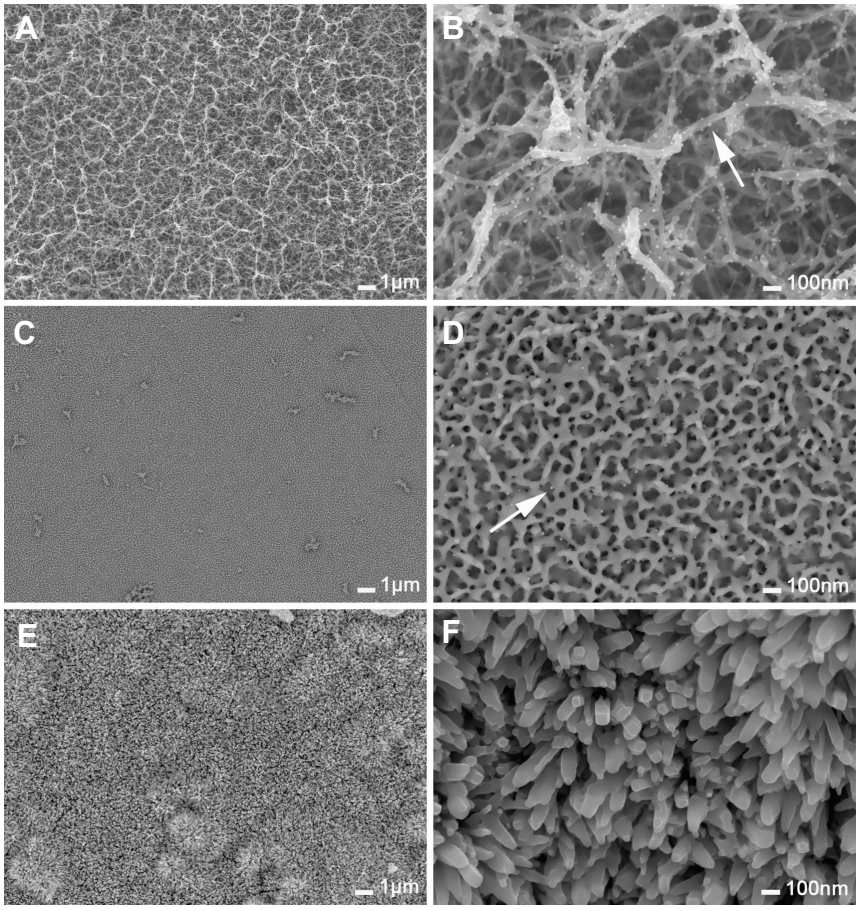

Figure 4 SEM morphology of the as-synthesized Ag@nanowire (**A**, **B**), Ag@nanotip (**C**, **D**), and Ag@nanorod (**E**, **F**) at low- and high-magnification, respectively.
Note: Arrows indicate Ag nanoparticles.
Abbreviation: SEM, scanning electron microscope.

TiO_2 films on titanium surface can affect the growth habit of Ag nanoparticles in TiO_2 films during the Ag–PIII process.

In fact, during the Ag–PIII process, the nanotopographies of TiO_2 films may affect the distribution of electric field around TiO_2 films and the structure of Ag plasma sheath around the films.[31] As a result, the difference in the nanotopographies of TiO_2 films may influence the nucleation, growth, and distribution of Ag nanoparticles in the TiO_2 nanofilms (Figure S1). This hypothesis may account for the observed results for the Ag-implanted TiO_2 nanowires, nanotips, and

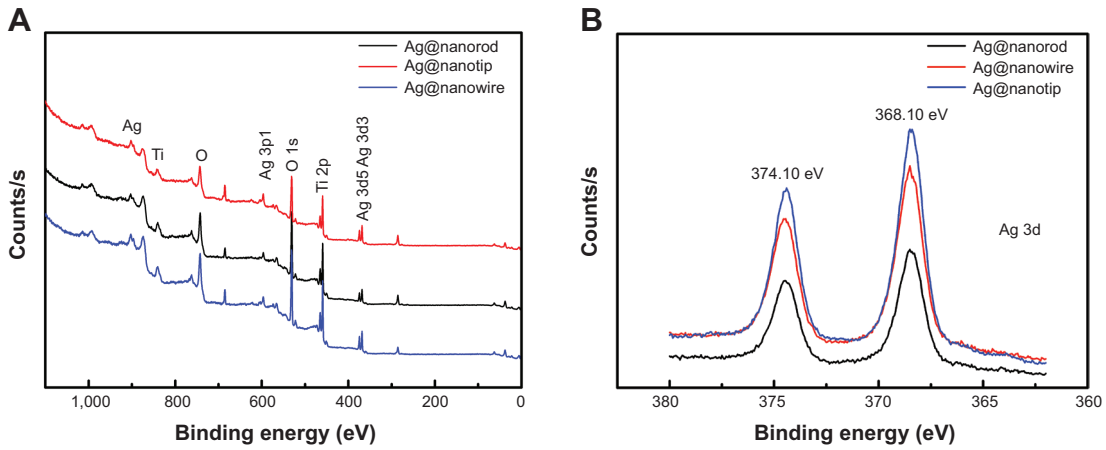

Figure 5 XPS full spectra (**A**) and the corresponding Ag 3d XPS spectra (**B**) of the Ag@nanowire, Ag@nanotip, and Ag@nanorod.
Abbreviation: XPS, X-ray photoelectron spectroscopy.

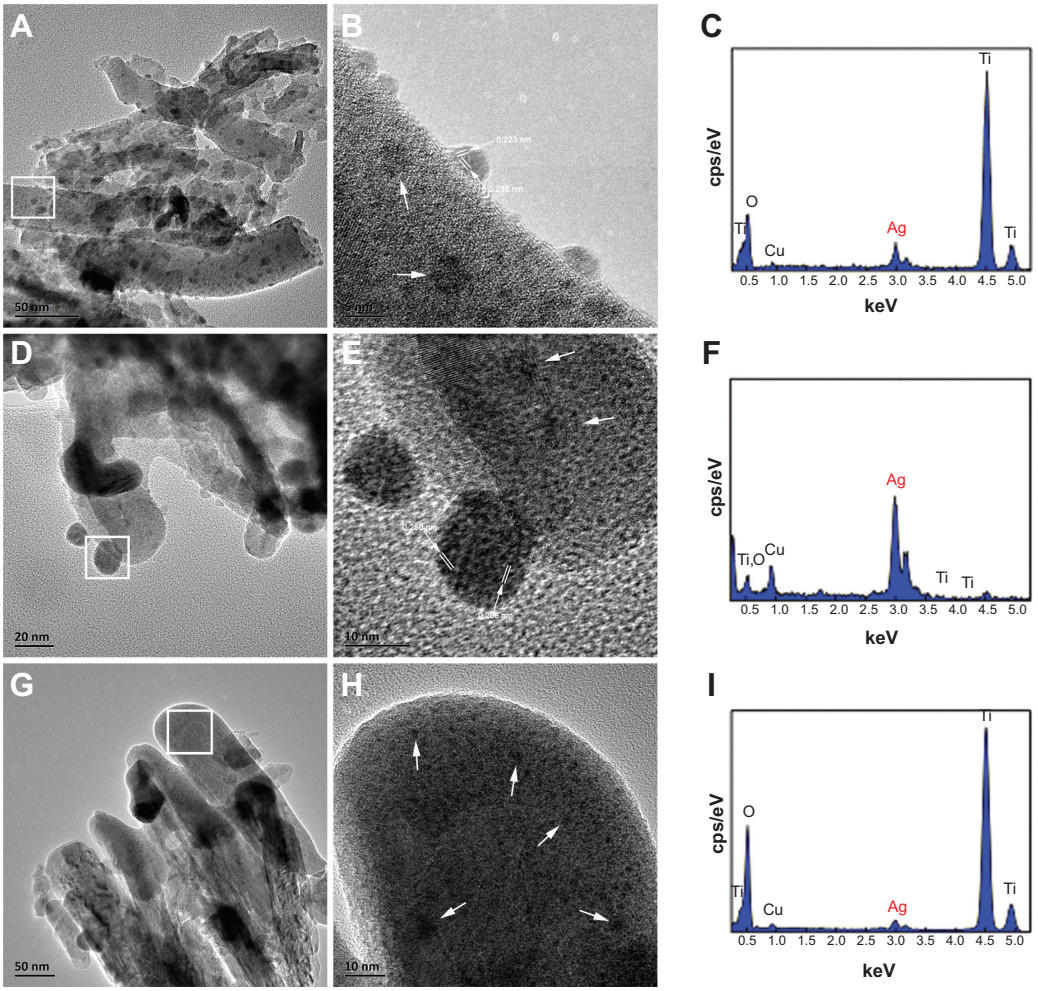

Figure 6 TEM analysis on the Ag-implanted samples: BF images obtained from Ag@nanowire (**A**), Ag@nanotip (**D**), and Ag@nanorod (**G**); (**B**), (**E**), and (**H**), the corresponding HRTEM lattice patterns of the encircled areas in (**A**), (**D**), and (**G**) respectively; (**C**), (**F**), and (**I**), the corresponding EDS results of the encircled areas in (**A**), (**D**), and (**G**), respectively.

Notes: Ag nanoparticles are indicated by large arrows, and lattice fringe spacings are shown with smaller arrows.

Abbreviations: TEM, transmission electron microscope; BF, bright field; HRTEM, high-resolution transmission electron microscope image; EDS, energy-dispersive X-ray spectroscopy.

nanorods. The exact mechanism remains unclear, and more work should be done to explain the mechanism in detail. On the basis of the XPS analysis, the contents of Ag element on the Ag@nanowire, Ag@nanotip, and Ag@nanorod are about 3.0%, 2.7%, and 1.9%, respectively. Up to now, the whole process aforementioned can be proposed and illustrated in Figure S1. Finally, as shown in Figure 4, three types of Ag-implanted TiO_2 nanotopographies were formed on the metallic titanium surface. And, the existing forms of Ag nanoparticles in the TiO_2 nanofilms will influence the Ag ions release and the related antimicrobial actions.

Ag ions release

The release behaviors of Ag ions from the Ag–PIII samples in fresh water are shown in Figure 7A. For the Ag@nanowire and Ag@nanotip, the Ag ions were obviously released from the Ag nanoparticles, especially for the Ag@nanowire. However, during the immersing period, no Ag ions were detected by the inductively coupled plasma mass spectrometry, indicating that Ag ions were not released from the Ag@nanorod. The XPS analysis was also conducted on the immersed samples after 7 days. As shown in Figure 7B, Ag element can still be detected on these samples in the form of metallic Ag (Figure 7C). Based on the analysis, the residual contents of Ag on the Ag@nanowire, Ag@nanotip, and Ag@nanorod are approximately 1.0%, 1.2%, and 1.8%, respectively. These observed results are quite consistent with the corresponding existing forms of Ag nanoparticles in TiO_2 nanofilms. Understandably, whether the Ag ions can be released will affect the antimicrobial actions of the Ag-implanted TiO_2 nanofilms.

Antimicrobial performance

It has been reported that the antibacterial behavior of Ag nanoparticles relies upon the availability of Ag ions,[38,39] and

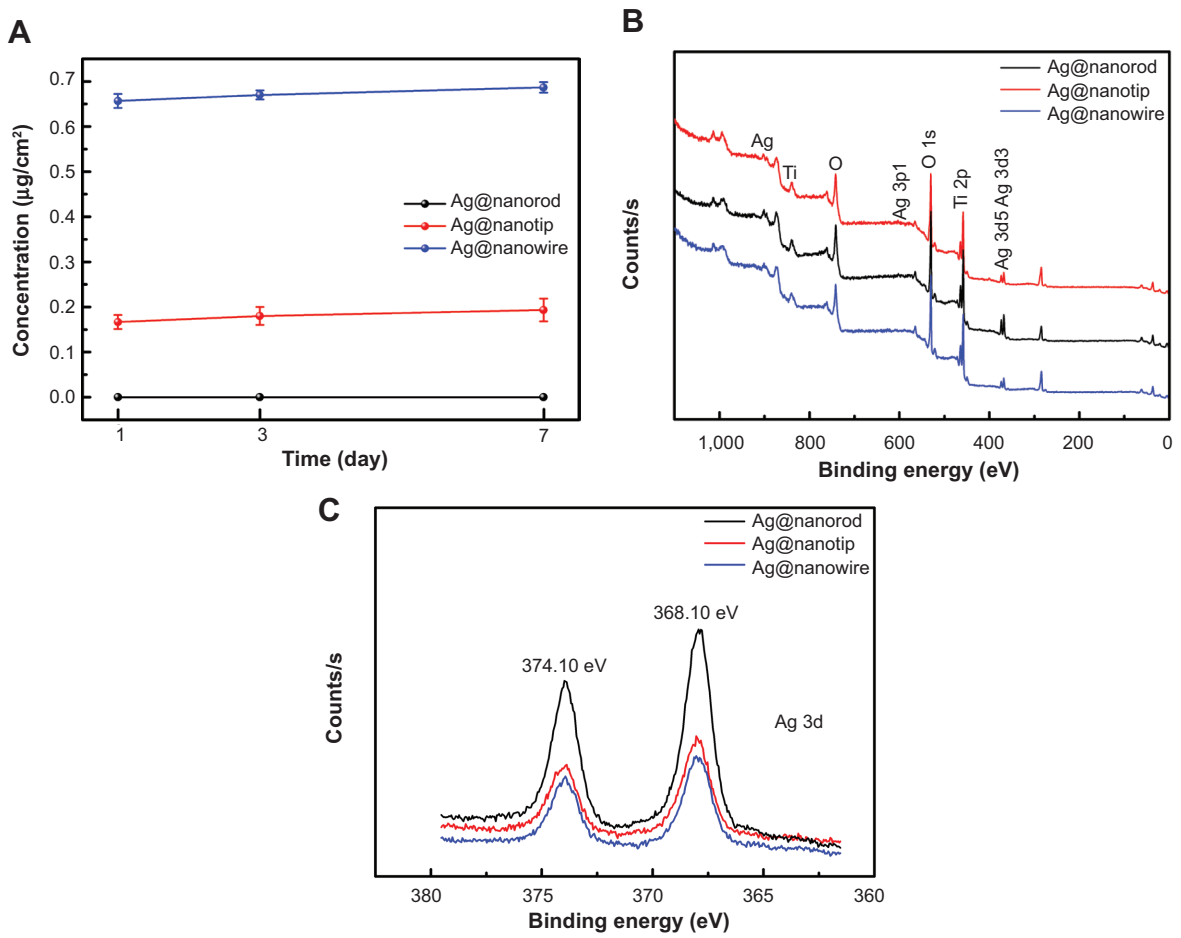

Figure 7 Concentration of Ag ions being released from the Ag@nanowire, Ag@nanotip, and Ag@nanorod after immersion in fresh water for different days (**A**), accompanied by the corresponding XPS full spectra (**B**), and Ag 3d XPS spectra (**C**) of these samples after immersion for 7 days.
Abbreviation: XPS, X-ray photoelectron spectroscopy.

the released amount of Ag ions in surrounding aqueous environment plays a key role in the antibacterial activity of Ag-loaded nano-TiO_2.[18] Furthermore, direct physical contact with the Ag nanoparticles can also induce bacteria death.[8,40,41] To evaluate the antibacterial ability of the as-prepared Ag–PIII specimens and to determine the antibacterial mechanism behind (including release killing and contact killing), the adhering microbes were dissociated off the surfaces and recultivated on an agar base on the bacterial counting method. Figure 8A shows the typical photographs of the bacterial colonies on the specimens, combined with the bacteria counting results. All the nanostructured TiO_2 surfaces can inhibit the proliferation of *E. coli* and *S. aureus* to some extent, especially for the nanorod TiO_2.

This could be attributed to the topography difference of the nano-TiO_2 surfaces. After Ag implantation, all the surfaces of Ag–PIII samples have the strong capability to suppress the growth of the two kinds of bacteria. The amounts of *E. coli* and *S. aureus* on the Ag-implanted TiO_2 nanofilms are notably decreased after 24 hours, as shown in Figure 8B and C.

To determine the reason, SEM method was used to observe the membrane morphology and integrity of both *E. coli* and *S. aureus* bacteria, as shown in Figure 9. Cell division dominates on the Cp Ti, while not the same on the surfaces of Ag–PIII specimens, revealing that the surfaces of Ag-implanted TiO_2 can kill the bacteria. Most of the *E. coli* cells cultured on the Cp Ti were at the stage of binary fission with rod shape (white arrow in Figure 9A1), which look smooth and without obvious damage. However, serious disruption of the cytoplasmic membrane can be seen on all the surfaces of Ag–PIII specimens, causing the lysis of the cell and the leakage of cytoplasma (white arrows in Figure 9B1, C1, and D1). This is also true for *S. aureus* cells, which present smooth and intact cytoplasmic membranes and produce abundant and continuous biofilms, implying that *S. aureus* can grow well on Cp Ti (white arrow in Figure 9A2).

Nevertheless, the phenomena of cell lysis and cytoplasma leakage are prevailing on all surfaces of the Ag–PIII samples (white arrows in Figure 9B2, C2, and D2), indicating that *S. aureus* bacteria cannot survive well on the surfaces of

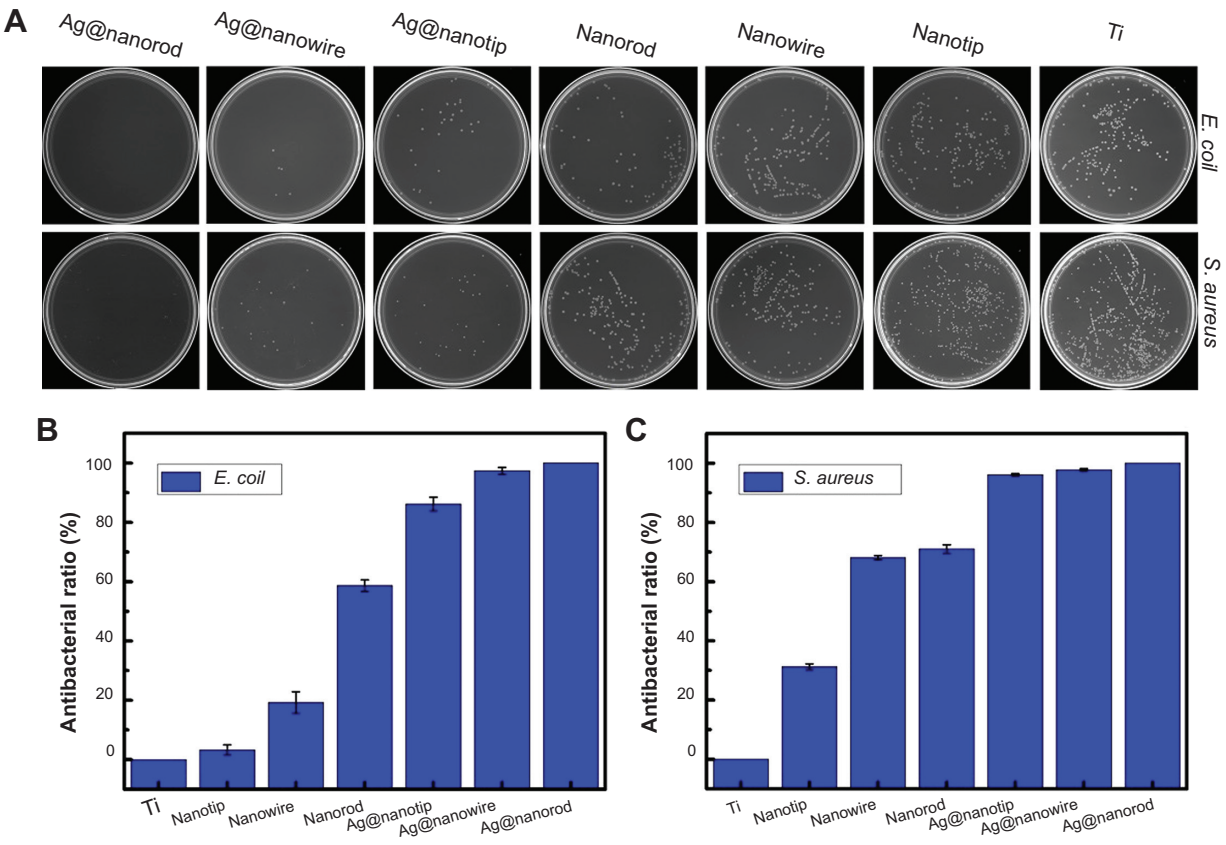

Figure 8 Typical photographs of recultivated *Escherichia coli* and *Staphylococcus aureus* colonies on agar (**A**) and the corresponding percentage reduction of bacteria colonies (**B**, **C**).
Note: All the data are expressed as means ± standard deviation (n=3).

Ag–PIII specimens. The observed results indicate that the death of both *E. coli* and *S. aureus* cells on the surfaces of Ag–PIII specimens can be ascribed to the damage of the microbial membrane integrity. Therefore, the Ag plasma-modified TiO_2 nanofilms have a significant antimicrobial function on both the bacteria, ie, Gram-negative *E. coli* and Gram-positive *S. aureus*.

Research focusing on the material characteristics of TiO_2 nanomaterials like topography, component, crystallinity, phase composition, etc, may shed light on the mechanism behind antibacterial actions (such as membrane penetration) and the release of Ag ions may affect the surface properties of TiO_2 and subsequent radical generation and lipid peroxidation on the surface.[11,42–44] In this work, the dissolution of

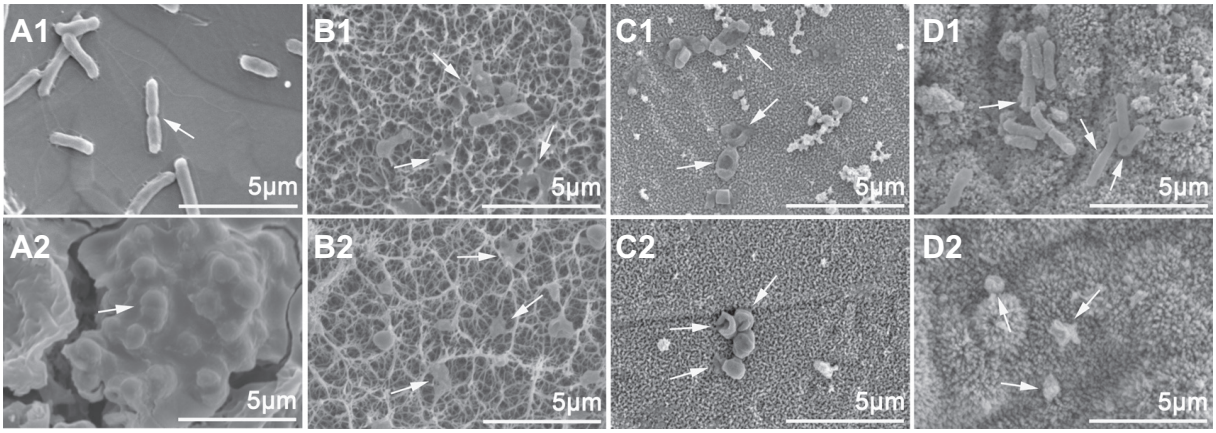

Figure 9 SEM morphology of the *Escherichia coli* (**A1-D1**, arrows) and *Staphylococcus aureus* (**A2-D2**, arrows) species seeded on the various surfaces (**A1-D1** and **A2-D2** represent Cp Ti, Ag@nanowire, Ag@nanotip, and Ag@nanorod, respectively) with the seeded bacteria concentration being 10^7 CFU/mL.
Abbreviations: SEM, scanning electron microscope; Cp, commercially pure; CFU, colony forming unit.

Ag nanoparticles release the antimicrobial Ag ions in the aqueous environment as Reaction 1, and partially contributes to the antimicrobial ability of the Ag–PIII surfaces through a release-killing way.[45]

$$\text{nano-Ag} \rightarrow Ag^{+} + e^{-} \quad (1)$$

The Ag ions released from the Ag nanoparticles can trigger inactivation of respiratory enzymes and interruption of electron transport[46,47] and interfere with permeability of microbial membrane and replication of DNA.[48] However, although the release amount of Ag^{+} ions had a significant difference (Figure 7A), the Ag-implanted TiO_2 nanofilms showed no significant difference here in the antimicrobial activity against both microbes (Figure 8B and C). For the Ag-implanted TiO_2 nanorods, understandably, it kills microbes via a direct physical contact that is, a sole contact-killing action. For the Ag-implanted TiO_2 nanowires and nanotips, they kill microbes via a two-level antimicrobial action comprising the release-killing ability and the contact-killing ability.

On the basis of the observed results, the contact-killing action is the main way to destroy microbes for all the Ag-implanted TiO_2 nanofilms. In fact, electrons can be captured and bounded by Ag nanoparticles owing to the building of the Schottky barrier at the interface of Ag/TiO_2, as Reaction 2, suppressing electron/hole recombination and thus inducing oxidation and reduction quantum yields.[49] The produced h^{+} holes will react with the on-surface OH^{-} ions or H_2O molecules and generate •OH radicals based on Reaction 3 or Reaction 4, or subsequently transform into H_2O_2 molecules, according to Reaction 5 since the •OH radicals have quite short lifespan.[50,51]

$$TiO_2 \xrightarrow{Ag} TiO_2(e^{-} + h^{+}) \quad (2)$$

$$h^{+} + OH^{-} \rightarrow \bullet OH \quad (3)$$

$$h^{+} + H_2O \rightarrow \bullet OH + H^{+} \quad (4)$$

$$\bullet OH + \bullet OH \rightarrow H_2O_2 \quad (5)$$

Consequently, •OH or H_2O_2 species accumulate near the cell membrane of bacteria and conduct the reaction of lipid peroxidation, that is, a contact-killing antibacterial way, destroying the membrane integrity of bacteria and eventually causing the inactivation of bacteria.[40] The hypothesized antimicrobial mechanism for Ag plasma-modified TiO_2 nanofilms can be illustrated in Figure 10. The aforementioned

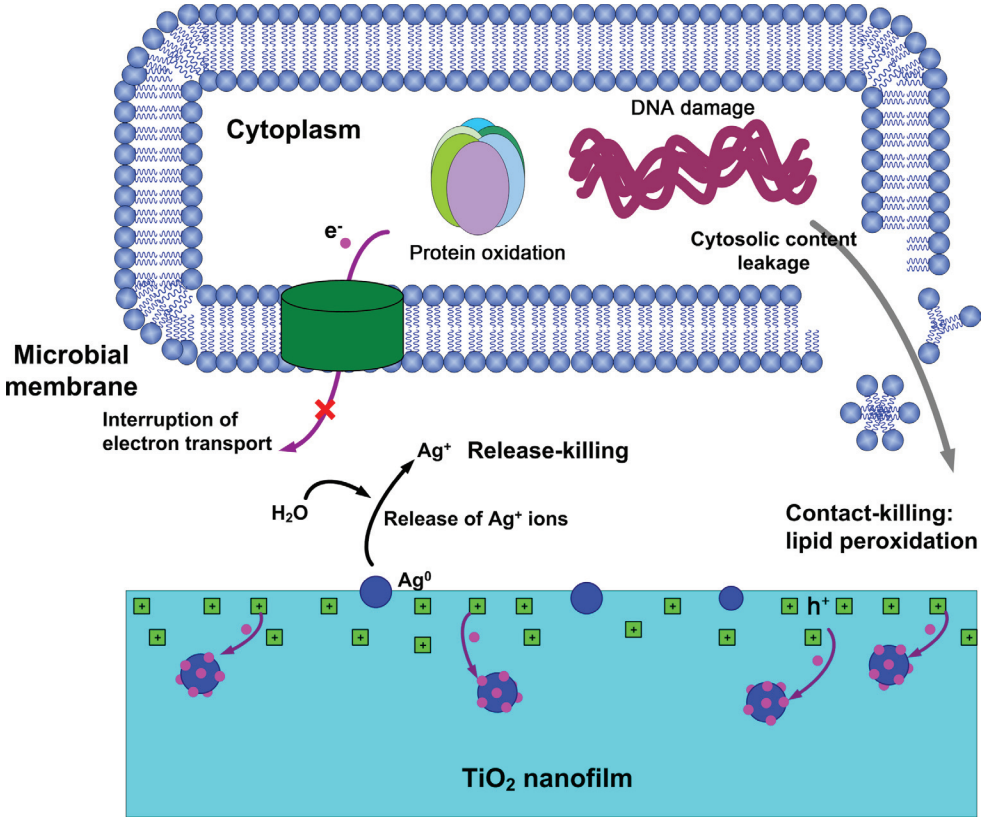

Figure 10 Illustration for antibacterial mechanism with both release-killing and contact-killing actions of Ag nanoparticles-loaded TiO_2 nanofilms in darkness.

explanation for the antibacterial behaviors of various Ag– PIII nano-TiO_2 surfaces is mainly a hypothesis, based on the observed experimental results. The true mechanism remains not clear. It is essential to do more studies to elucidate the mechanism behind in detail. It is considered that, by optimizing the PIII parameters, Ag nanoparticles with different existing forms, including the exposed ones on the surface and the embedded ones beneath the surface, are incorporated with TiO_2 nanorod film, followed by the antibacterial experiment to further investigate the antibacterial ability.

Conclusion

The Ag plasma-modified nanostructured TiO_2 films (including nanorod, nanotip, and nanowire topographies) were successfully prepared on the titanium surface via a combination of hydrothermal method and Ag–PIII technique. Compared to the acid-etched titanium, the nanostructured TiO_2 films possess some bacteriostatic effect toward both Gram-negative *E. coli* and Gram-positive *S. aureus*. The existing forms of the Ag nanoparticles show differently in the TiO_2 films with different nanotopographies, which results in the significantly different release behaviors of Ag ions. However, the antimicrobial evaluation tests show no significant difference against both microbes. The antimicrobial actions of the Ag@TiO_2 system here consist of two paths, that is, the contact killing and the release killing. Nevertheless, on the basis of the obtained results, the contact-killing action should be considered as the main way to destroy microbes for all the Ag plasma-modified TiO_2 nanofilms. This study provides insight to the antimicrobial design of Ti-based implants surfaces.

Acknowledgments

The authors received joint financial support from: the National Basic Research Program of China (973 Program, 2012CB933600); the National Natural Science Foundation of China (31100675, 51071168, and 81271704); the Shanghai Science and Technology R&D Fund under grant 11JC1413700.

Disclosure

The authors report no conflicts of interest in this work.

References

1. Liu X, Chu PK, Ding C. Surface nano-functionalization of biomaterials. *Materials Science and Engineering: R: Reports*. 2010;70(3–6):275–302.
2. Geetha M, Singh AK, Asokamani R, Gogia AK. Ti based biomaterials, the ultimate choice for orthopaedic implants – A review. *Progress in Materials Science*. 2009;54(3):397–425.
3. Monteiro DR, Gorup LF, Takamiya AS, Ruvollo-Filho AC, de Camargo ER, Barbosa DB. The growing importance of materials that prevent microbial adhesion: antimicrobial effect of medical devices containing silver. *Int J Antimicrob Agents*. 2009;34(2):103–110.
4. Hetrick EM, Schoenfisch MH. Reducing implant-related infections: active release strategies. *Chem Soc Rev*. 2006;35(9):780–789.
5. Wu S, Liu X, Yeung A, et al. Plasma-modified biomaterials for self-antimicrobial applications. *ACS Appl Mater Interfaces*. 2011;3(8):2851–2860.
6. Costerton JW, Stewart PS, Greenberg EP. Bacterial biofilms: a common cause of persistent infections. *Science*. 1999;284(5418):1318–1322.
7. Kelland K. "Super Superbug" NDM-1 Spreads in Europe. *Clinical Infectious Diseases*. 2011;52(4):I–II. doi: 10.1093/cid/ciq232.
8. Chernousova S, Epple M. Silver as antibacterial agent: ion, nanoparticle, and metal. *Angew Chem Int Ed Engl*. 2013;52(6):1636–1653.
9. Li J, Wang G, Zhu H, et al. Antibacterial activity of large-area monolayer graphene film manipulated by charge transfer. *Sci Rep*. 2014;4:4359.
10. Visai L, De Nardo L, Punta C, et al. Titanium oxide antibacterial surfaces in biomedical devices. *Int J Artif Organs*. 2011;34(9):929–946.
11. Henderson MA. A surface science perspective on TiO_2 photocatalysis. *Surface Science Reports*. 2011;66(6–7):185–297.
12. Takai A, Kamat PV. Capture, store, and discharge. Shuttling photogenerated electrons across TiO_2-silver interface. *ACS Nano*. 2011;5(9):7369–7376.
13. Li Q, Li YW, Liu Z, Xie R, Shang JK. Memory antibacterial effect from photoelectron transfer between nanoparticles and visible light photocatalyst. *J Mater Chem*. 2010;20(6):1068–1072.
14. Wu P, Imlay JA, Shang JK. Mechanism of Escherichia coli inactivation on palladium-modified nitrogen-doped titanium dioxide. *Biomaterials*. 2010;31(29):7526–7533.
15. Hurdle JG, O'Neill AJ, Chopra I, Lee RE. Targeting bacterial membrane function: an underexploited mechanism for treating persistent infections. *Nat Rev Microbiol*. 2011;9(1):62–75.
16. Allison KR, Brynildsen MP, Collins JJ. Metabolite-enabled eradication of bacterial persisters by aminoglycosides. *Nature*. 2011;473(7346):216–220.
17. Ren N, Li R, Chen L, et al. In situ construction of a titanate-silver nanoparticle-titanate sandwich nanostructure on a metallic titanium surface for bacteriostatic and biocompatible implants. *J Mater Chem*. 2012;22(36):19151–19160.
18. Juan L, Zhimin Z, Anchun M, Lei L, Jingchao Z. Deposition of silver nanoparticles on titanium surface for antibacterial effect. *Int J Nanomedicine*. 2010;5:261–267.
19. Zhao L, Wang H, Huo K, et al. Antibacterial nano-structured titania coating incorporated with silver nanoparticles. *Biomaterials*. 2011;32(24):5706–5716.
20. Xiao W, Xu J, Liu X, Hu Q, Huang J. Antibacterial hybrid materials fabricated by nanocoating of microfibril bundles of cellulose substance with titania/chitosan/silver-nanoparticle composite films. *Journal of Materials Chemistry B*. 2013;1(28):3477–3485.
21. Mahanta N, Valiyaveettil S. In situ preparation of silver nanoparticles on biocompatible methacrylated poly(vinyl alcohol) and cellulose based polymeric nanofibers. *RSC Advances*. 2012;2(30):11389–11396.
22. Huo D, Gao J, Guo B, et al. Silver nanoshells as tri-mode bactericidal agents integrating long term antibacterial, photohyperthermia and triggered Ag^+ release capabilities. *RSC Advances*. 2013;3(27):10632–10638.
23. Liu X, Chu PK, Ding C. Surface modification of titanium, titanium alloys, and related materials for biomedical applications. *Materials Science and Engineering: R: Reports*. 2004;47(3–4):49–121.
24. Zheng Y, Li J, Liu X, Sun J. Antimicrobial and osteogenic effect of Ag-implanted titanium with a nanostructured surface. *Int J Nanomedicine*. 2012;7:875–884.
25. Zhang W, Luo Y, Wang H, Jiang J, Pu S, Chu PK. Ag and Ag/N2 plasma modification of polyethylene for the enhancement of antibacterial properties and cell growth/proliferation. *Acta Biomater*. 2008;4(6):2028–2036.

26. Zhang W, Luo Y, Wang H, Pu S, Chu PK. Biocompatibility of silver and copper plasma doped polyethylene. *Surface and Coatings Technology*. 2009;203(17–18):2550–2553.
27. Wang H, Kwok DT, Xu M, et al. Tailoring of mesenchymal stem cells behavior on plasma-modified polytetrafluoroethylene. *Adv Mater*. 2012;24(25):3315–3324.
28. Cao H, Liu X, Meng F, Chu PK. Biological actions of silver nanoparticles embedded in titanium controlled by micro-galvanic effects. *Biomaterials*. 2011;32(3):693–705.
29. Hou W, Liu Z, Pavaskar P, Hung WH, Cronin SB. Plasmonic enhancement of photocatalytic decomposition of methyl orange under visible light. *J Catal*. 2011;277(2):149–153.
30. Stepanov AL. Applications of ion implantation for modification of TiO_2: a review. *Reviews on Advanced Materials Science*. 2012;30(2):150–165.
31. Qian S, Cao H, Liu X, Ding C. Nanotube array controlled carbon plasma deposition. *Appl Phys Lett*. 2013;102(24):243109.
32. Hu H, Zhang W, Qiao Y, Jiang X, Liu X, Ding C. Antibacterial activity and increased bone marrow stem cell functions of Zn-incorporated TiO_2 coatings on titanium. *Acta Biomater*. 2012;8(2):904–915.
33. Yun JH, Wong RJ, Ng YH, Du A, Amal R. Combined electrophoretic deposition-anodization method to fabricate reduced graphene oxide-TiO_2 nanotube films. *RSC Advances*. 2012;2(21):8164–8171.
34. Han Y, Chen D, Sun J, Zhang Y, Xu K. UV-enhanced bioactivity and cell response of micro-arc oxidized titania coatings. *Acta Biomaterialia*. 2008;4(5):1518–1529.
35. Wang L, Xue Z, Liu X, Liu B. Transfer of asymmetric free-standing TiO_2 nanowire films for high efficiency flexible dye-sensitized solar cells. *RSC Advances*. 2012;2(20):7656–7659.
36. Wang X, Yu JC, Ho C, Mak AC. A robust three-dimensional mesoporous Ag/TiO_2 nanohybrid film. *Chem Commun (Camb)*. 2005;(17):2262–2264.
37. Wang D, Zhou Z-H, Yang H, et al. Preparation of TiO_2 loaded with crystalline nano Ag by a one-step low-temperature hydrothermal method. *J Mater Chem*. 2012;22(32):16306–16311.
38. Chen X, Schluesener HJ. Nanosilver: a nanoproduct in medical application. *Toxicol Lett*. 2008;176(1):1–12.
39. Eckhardt S, Brunetto PS, Gagnon J, Priebe M, Giese B, Fromm KM. Nanobio silver: its interactions with peptides and bacteria, and its uses in medicine. *Chem Rev*. 2013;113(7):4708–4754.
40. Su HL, Chou CC, Hung DJ, et al. The disruption of bacterial membrane integrity through ROS generation induced by nanohybrids of silver and clay. *Biomaterials*. 2009;30(30):5979–5987.
41. Cao H, Liu X. Activating titanium oxide coatings for orthopedic implants. *Surf Coat Technol*. 2013;233:57–64.
42. Liu X, Chen G, Erwin JG, Su C. Silicon impurity release and surface transformation of TiO_2 anatase and rutile nanoparticles in water environments. *Environ Pollut*. 2014;184:570–578.
43. Fujishima A, Zhang X, Tryk DA. TiO_2 photocatalysis and related surface phenomena. *Surf Sci Rep*. 2008;63(12):515–582.
44. Diebold U. The surface science of titanium dioxide. *Surf Sci Rep*. 2003;48(5):53–229.
45. Morones JR, Elechiguerra JL, Camacho A, et al. The bactericidal effect of silver nanoparticles. *Nanotechnology*. 2005;16(10):2346–2353.
46. Matsumura Y, Yoshikata K, Kunisaki S, Tsuchido T. Mode of bactericidal action of silver zeolite and its comparison with that of silver nitrate. *Appl Environ Microbiol*. 2003;69(7):4278–4281.
47. Holt KB, Bard AJ. Interaction of silver (I) ions with the respiratory chain of Escherichia coli: an electrochemical and scanning electrochemical microscopy study of the antimicrobial mechanism of micromolar Ag^+. *Biochemistry*. 2005;44(39):13214–13223.
48. Feng QL, Wu J, Chen GQ, Cui FZ, Kim TN, Kim JO. A mechanistic study of the antibacterial effect of silver ions on Escherichia coli and Staphylococcus aureus. *J Biomed Mater Res*. 2000;52(4):662–668.
49. Jakob M, Levanon H, Kamat PV. Charge Distribution between UV-Irradiated TiO_2 and Gold Nanoparticles: Determination of Shift in the Fermi Level. *Nano Lett*. 2003;3(3):353–358.
50. Sunada K, Kikuchi Y, Hashimoto K, Fujishima A. Bactericidal and Detoxification Effects of TiO_2 Thin Film Photocatalysts. *Environ Sci Technol*. 1998;32(5):726–728.
51. Maness PC, Smolinski S, Blake DM, Huang Z, Wolfrum EJ, Jacoby WA. Bactericidal activity of photocatalytic TiO(2) reaction: toward an understanding of its killing mechanism. *Appl Environ Microbiol*. 1999;65(9):4094–4098.

Supplementary materials

Qualitatively, the nucleation and growth behavior of Ag nanoparticles in TiO_2 nanofilms can be comprehended by the classical nucleation theory.[1] The excess free energy (ΔG) can be described by Equation S1,[2]

$$\Delta G = 4\pi r^2 \gamma - \frac{4}{3}\pi r^3 \frac{RT \ln S}{V_m} \quad \text{(S1)}$$

in which: r, the cluster radius; γ, the surface tension of the cluster; RT, the product of ideal gas constant (R) and the absolute temperature (T); S, the ratio of the solute concentrations at saturation and equilibrium conditions; and V_m, the molar volume of the bulk crystal.

When $S > 1$ (supersaturated condition), the increase of r value will result in the decrease of ΔG value, making the clusters more stable. The critical radius of a nucleus (r^*) at supersaturated condition can be determined by setting $d\Delta G/dr = 0$ as Equation S2, at which ΔG^* is maximum,

$$r^* = \frac{2\gamma V_m}{RT \ln S} \quad \text{(S2)}$$

Based on Equation S2, r^* is in inverse ratio to lnS, revealing that an increase in lnS procures a decrease in minimum nucleus radius (r^*). Thus, when the concentration of Ag atoms exceeds the solubility limit of metal atoms in TiO_2 nanofilm matrix, the system will relax by the nucleation and growth of the Ag nanoparticles.

During the Ag–PIII process, energetic Ag plasma could be blocked by the substrate, and part of the kinetic energy will be transformed into heat energy in the ultrashort period in restricted regions, which is called the atomic scale heating.[3]

In the present situation, cathodic-arc Ag ions undergo three acceleration zones. The first zone is beside the cathode spot, generating the initial ion kinetic energy (E_k). The second zone is in the space charge sheath between the Ag plasma and TiO_2 nanofilm surface. Additional kinetic energy QeV_b is acquired for the ion of charge state Q with a negative bias voltage (V_b) applied to the TiO_2 nanofilm, where e is the elementary charge. The third zone is in the nanoscale vicinity of TiO_2 nanofilm matrix where image charge acceleration emerges and procures kinetic energy (E_i). Besides, Ag ions also possess substantial potential energy which contains ionization energy E_Q, cohesive energy E_c, and excitation energy of bound electrons E_e. The ionization energy (E_Q) is defined as the essential energy to remove a bound electron from an ion with charge state Q, generating an ion with charge state $Q+1$. Thus, the ionization energy E_Q of a triply charged Ag ion should be the summation of all the three ionization steps as follows in Equation S3,[3]

$$E_Q^{sum} = \sum_{i=0}^{Q-1} E_Q^i \quad \text{(S3)}$$

The general formula to express the total energy of an Ag ion is given by Equation S4,[3]

$$E = E_k + QeV_b + E_i + E_c + E_e + \sum_{i=0}^{Q-1} E_Q^i \quad \text{(S4)}$$

The previously reported and the presently calculated compositions of the total energy for the Ag ion reaching TiO_2 nanofilm matrix are listed in Table S1.

Here, the mean charge state (Q) equals to approximately 2.[4] The donation of electronic excitation energies (E_e) is comparatively slight and negligible in Table S1.[5] The kinetic energy E_i induced by image charge acceleration is calculated on the basis of Equation S5,[6]

$$E_i = \frac{W}{2} \sum_{j=0}^{Q-1} \frac{2(Q-j)-1}{\sqrt{8(Q-j)+2}} \quad \text{(S5)}$$

Considering the work function (W) of the TiO_2 nanofilm matrix, the value of W is about 4.13 eV,[7] and the kinetic energy E_i can be estimated, approximately 2.11 eV.

On the basis of the data in Table S1, the total energy gain of an individual Ag ion is much higher than the minimum displacement energy ranging from 10–40 eV,[3] which thus can potentially remove and dislodge stationary Ag atoms in the TiO_2 nanofilm matrix, which may explain the observed results for the Ag-implanted TiO_2 nanowires and nanotips. However, this explanation cannot completely meet the situation for the Ag-implanted TiO_2 nanorods. The nanorod topography of TiO_2 film may influence the electric field distribution and Ag plasma sheath structure around the TiO_2 film during the Ag-PIII process, thus affecting the nucleation, growth, and distribution of Ag nanoparticles in the TiO_2 nanorods.

Table S1 Energy gain (in eV) of an Ag ion with a mean charge state of $Q \approx 2$

E_k	QeV_b	E_i	E_c	E_e	E_Q^{Sum}
69.00[α]	3.00 E4[β]	2.11[β]	2.95[α]	≈0[γ]	29.1[α]

Notes: [α]from reference 3; [β]calculated with V_s =15 kV, which is approximate to the bias voltage in the present discussion; [γ]from reference 5.

Abbreviations: E_Q, ionization energy; E_i, kinetic energy; E_c, cohesive energy; E_e, excitation energy of bound electrons; V_b, negative bias voltage; e, elementary charge; Q, charge state.

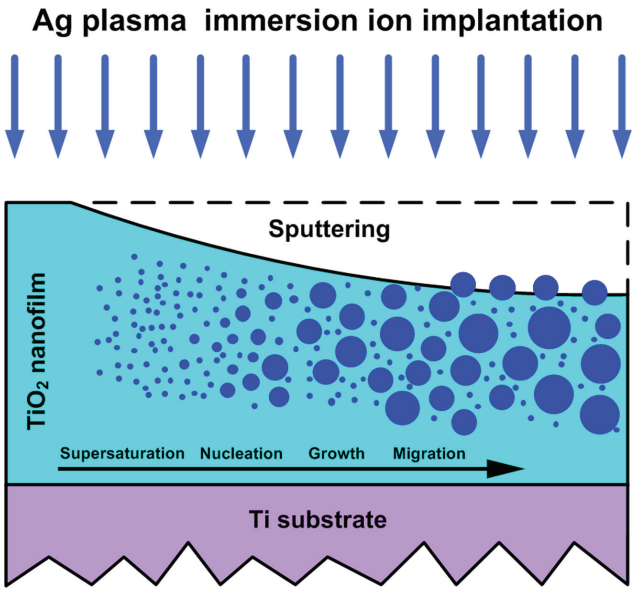

Figure S1 Proposed schematic illustration of basic physical processes (from left to right) involved in the formation of Ag nanoparticles in TiO_2 nanofilms during the Ag–PIII process.
Abbreviation: PIII, plasma immersion ion implantation.

References

1. Stepanov AL. Applications of ion implantation for modification of TiO_2: a review. *Reviews on Advanced Materials Science*. 2012;30(2):150–165.
2. Christian JW. *The Theory of Transformations in Metals and Alloys*. 3rd ed. Oxford, UK: Elsevier Science Ltd; 2002.
3. Anders A. Atomic scale heating in cathodic arc plasma deposition. *Appl Phys Lett*. 2002;80(6):1100–1102.
4. Brown IG. Vacuum arc ion sources. *Rev Sci Instrum*. 1994;65(10):3061–3081.
5. Anders A. *Cathodic Arcs: From Fractal Spots to Energetic Condensation*. New York, NY, USA: Springer Science+Business Media, LLC; 2008.
6. Burgdörfer J, Meyer F. Image acceleration of multiply charged ions by metallic surfaces. *Phys Rev A*. 1993;47(1):R20–R22.
7. Imanishi A, Tsuji E, Nakato Y. Dependence of the Work Function of TiO_2 (Rutile) on Crystal Faces, Studied by a Scanning Auger Microprobe. *J Phys Chem A*. 2007;111(5):2128–2132.